Proceedings of the 2006 IEEE International Conference on Robotics and Automation
Orlando, Florida - May 2006

Human Like Vision Using Conformal Geometric Algebra

Eduardo Bayro-Corrochano and David Gonzalez-Aguirre
CINVESTAV Unidad Guadalajara,
Department of Electrical Engineering and Computer Science,
Guadalajara, Mexico,
edb@gdl.cinvestav.mx, dgonzalez@gdl.cinvestav.mx

***Abstract*— In this paper we introduce a conformal model for stereoscopic perception systems. This model fuses stereoscopic views using an extended 3D horopter concept. This model is suitable for building a powerful binocular head for humanoids, intuitive man-machine interfaces and advanced 3D automated visual inspection.**

I. Introduction

The authors introduce a novel approach for building stereoscopic perception systems. The standard 2D horopter concept is reformulated now as a 3D horopter using conformal geometric algebra. In this mathematical system the 3D visual space is represented as a family of horopter spheres which together with their Poncelet points lead remarkably to a 3D log-polar representation of the visual space. There is quite abundant research activity on image processing using 2D log-polar schemes with either monocular or stereo systems [1], [5]. However this kind of work is representing basically the cartesian world using polar coordinates, and it fails to fuse the data of the two cameras of the stereoscopic vision system in a single framework. We believe that our human-like computational scheme looks promising for the processing of 3D visual space data. The structure of this paper comprises the following sections. Section two gives a brief introduction to conformal geometric algebra. Section three describes the conformal model for stereoscopic perception and provides insights in the implementation details which supports a kind of human processing of the visual perception. We show an applicatiuon using real images. The conclusions are given in section four.

II. Geometric Algebra: An Outline

Let $\mathcal{G}_n$ denote the geometric algebra of n-dimensions, this is a graded linear space. As well as vector addition and scalar multiplication we have a non-commutative product which is associative and distributive over addition – this is the *geometric* or *Clifford product*. A further distinguishing feature of the algebra is that any vector squares to give a scalar. The geometric product of two vectors a and b is written ab and can be expressed as a sum of its symmetric and antisymmetric parts

$$ab = a \cdot b + a \wedge b, \tag{1}$$

The inner product of two vectors is the standard *scalar* or *dot* product and produces a scalar. The outer or wedge product of two vectors is a new quantity which we call a *bivector*. We think of a bivector as a oriented area in the plane containing a and b, formed by sweeping a along b. Thus, $b \wedge a$ will have the opposite orientation making the wedge product anti-commutative. The outer product is immediately generalizable to higher dimensions – for example, $(a \wedge b) \wedge c$, a *trivector*, is interpreted as the oriented volume formed by sweeping the area $a \wedge b$ along vector c. The outer product of k vectors is a k-vector or k-blade, and such a quantity is said to have *grade* k. A *multivector* (linear combination of objects of different type) is *homogeneous* if it contains terms of only a single grade.

A. The Geometric algebra of n-D space

In this paper we will specify a geometric algebra $\mathcal{G}_n$ of the n dimensional space by $\mathcal{G}_{p,q,r}$, where p, q and r stand for the number of basis vector which squares to 1, -1 and 0 respectively and fulfill $n = p + q + r$. We will use e_i to denote the vector basis i. In a Geometric algebra $G_{p,q,r}$, the geometric product of two basis vector is defined as

$$e_i e_j = \begin{cases} 1 & f \quad i = j \in 1, \cdots, \\ -1 & f \quad i = j \in \ +1, \cdots, \ + \\ 0 & f \quad i = j \in \ + \ +1, \cdots, \ + \ + \ . \\ e_i \wedge e_j & f \quad i \neq j \end{cases}$$

This leads to a basis for the entire algebra:

$$\{1\}, \{e_i\}, \{e_i \wedge e_j\}, \{e_i \wedge e_j \wedge e_k\}, \ldots, \{e_1 \wedge e_2 \wedge \ldots \wedge e_n\} \tag{2}$$

Any multivector can be expressed in terms of this basis. In the n-D space there are multivectors of grade 0 (scalars), grade 1 (vectors), grade 2 (bivectors), grade 3 (trivectors), etc... up to grade n. Any two such multivectors can be multiplied using the geometric product. Consider two multivectors $\boldsymbol{A_r}$ and $\boldsymbol{B_s}$ of grades $\boldsymbol{r}$ and $\boldsymbol{s}$ respectively. The geometric product of $\boldsymbol{A_r}$ and $\boldsymbol{B_s}$ can be written as

$$\boldsymbol{A_r B_s} = \langle \boldsymbol{AB} \rangle_{\boldsymbol{r+s}} + \langle \boldsymbol{AB} \rangle_{\boldsymbol{r+s-2}} + \ldots + \langle \boldsymbol{AB} \rangle_{\boldsymbol{|r-s|}} \tag{3}$$

where $\langle \boldsymbol{M} \rangle_{\boldsymbol{t}}$ is used to denote the $\boldsymbol{t}$-grade part of multivector $\boldsymbol{M}$, e.g. consider the geometric product of two vectors $\boldsymbol{ab} = \langle \boldsymbol{ab} \rangle_{\boldsymbol{0}} + \langle \boldsymbol{ab} \rangle_{\boldsymbol{2}} = \boldsymbol{a \cdot b + a \wedge b}$.

B. Conformal Geometry

Geometric algebra $G_{4,1}$ can be used to treat conformal geometry. To see how this is possible, we follow the same formulation presented in [7] and show how the Euclidean

vector space $\mathbb{R}^3$ is represented in $\mathbb{R}^{4,1}$. This space has orthonormal vector basis given by $\{e_i\} i \in \{1,2,3,4 \text{ and } 5\}$ and $e_{ij} = e_i \wedge e_j$ are bivectorial basis, where e_{23}, e_{31} and e_{12} correspond to the Hamilton basis (i,j,k). The unit Euclidean pseudo-scalar $I_e := e_1 \wedge e_2 \wedge e_3$, a unit Conformal pseudo-scalar $I_c := I_e E$ where the bivector $E := e_4 \wedge e_5 = e_4 e_5$, these are used to compute the inverse and duals of multivectors.

The two basis added e_4 and e_5 square to 1 and -1 respectively, and this are used to define two null vectors

$$e_0 = \frac{e_4 - e_5}{2} \tag{4}$$

and

$$e_\infty = e_4 + e_5, \tag{5}$$

where e_0 is interpreted as the origin of the coordinate system and e_∞ is the point at infinity. Then a point $x_e \in \mathbb{R}^3$ in conformal spaces is expressed by

$$x_c \quad = \quad x_e + \frac{1}{2} x_e^2 e_\infty + e_o. \tag{6}$$

The equation of a sphere of radius ρ centered at point $p_e \in \mathbb{R}^n$ can be written as

$$(x_e - p_e)^2 = \rho^2. \tag{7}$$

Since $x_c \cdot y_c = -\frac{1}{2}(\mathbf{x}_e - \mathbf{y}_e)^2$, we can rewrite the formula above in terms of homogeneous coordinates as.

$$x_c \cdot p_c = -\frac{1}{2}\rho^2. \tag{8}$$

Since $x_c \cdot e_\infty = -1$ we can factor the expression above to

$$x_c \cdot (p_c - \frac{1}{2}\rho^2 e_\infty) = 0. \tag{9}$$

Which finally yields the simplified equation for the sphere as

$$s = p_c - \frac{1}{2}\rho^2 e_\infty. \tag{10}$$

Note from this equation that a point is just a sphere with zero radius. Alternatively, the dual of the sphere is represented as 4-vector $s^* = sI_c$. The advantage of the dual form is that the sphere can be directly computed from four points (in 3D) as

$$s^* = x_{c_1} \wedge x_{c_2} \wedge x_{c_3} \wedge x_{c_4}. \tag{11}$$

If we replace one of these points for the point at infinity we get the equation of a plane

$$\pi^* = x_{c_1} \wedge x_{c_2} \wedge x_{c_3} \wedge e_\infty. \tag{12}$$

So that π becomes in the standard form

$$\pi \quad = I_c \pi^* = \quad n + d e_\infty \tag{13}$$

Where n is the normal vector and d represents the Hesse distance.

C. Circles and Lines

A circle z can be regarded as the intersection of two spheres s_1 and s_2 as $z = (s_1 \wedge s_2)$. The dual form of the circle (in 3D) can be expressed by three points lying on it as

$$z^* = x_{c_1} \wedge x_{c_2} \wedge x_{c_3}. \tag{14}$$

Similar to the case of planes, lines can be defined by circles passing through the point at infinity as:

$$L^* = x_{c_1} \wedge x_{c_2} \wedge e_\infty. \tag{15}$$

D. Rigid motion in the conformal geometric algebra.

In $G_{4,1}$ the rotations are represented by rotors $R = \exp(\frac{\theta}{2} l)$. Where the bivector l is the screw of rotation axis and the amount of rotation is given by the angle θ. An entity can be rotated by multiplying from the left with the rotor R and from the right with its reverse $\widetilde{R}$ (e.g., $x' = Rx\widetilde{R}$).

One entity can be translated with respect to a translation vector t using the translator $T = 1 + \frac{et}{2} = \exp(\frac{et}{2})$. The translation takes place by multiplying from the left with the translator T and from the right with $\widetilde{T}$ (e.g., $Tx\widetilde{T}$).

To express the rigid motion of an object we can apply a rotor and a translator simultaneously, this composition is equals to a motor $M = TR$. We apply the motor similarly as the rotor and the translator (e.g. $x = Mx\widetilde{M}$). Surprisingly this formulation of the rigid motion can be applied not only to lines and points but also to planes, circles and spheres.

III. Conformal Model for Stereoscopic Perception Systems

Now we explain how we developed a conformal model for representing 3D information of the visual space. We start explaining the relationship between the horopter and our conformal model. Thereafter we describe how we build a real time system using our model.

A. Horopter and the conformal model

The horopter is the 3D geometric locus in space where an object has to be placed in order to stimulate exactly two points in correspondence in the left and right retinas of a biologic binocular vision system [4]. In Figure 1.c-d we see a horopter depending of an azimuth angle κ. In other words the horopter represents a set of points that cause minimal (almost zero) disparity on the retinas. We draw the horopter tracing an arc through the fixation point and the nodal points of the two retinas, see Figure 1.a. The theoretical horopter is known as the Vieth-Müller circle. Note that each fixation distance has its own Vieth-Müller circle. According to this theoretical view, the following assumptions can be made: each retina may be a perfect circle, both retinas are of the same size, corresponding points are perfectly matched in their retina locations, and points in correspondence are evenly spaced across the nasal and temporal retinas of the right and left eyes.

If an object is located in either side of the horopter, a small amount of disparity is caused by the eyes. The brain analyzes this disparity and computes the relative distance of the object with respect to the horopter. The sensation of

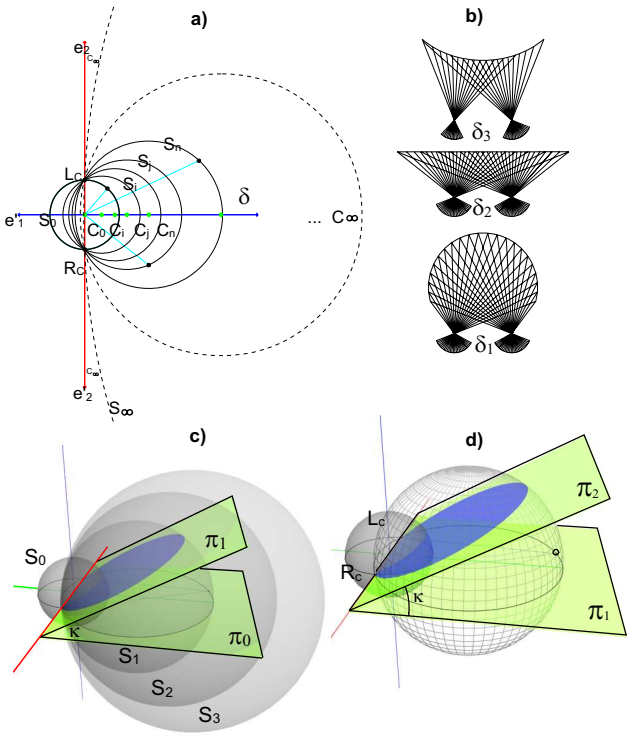

Fig. 1. a) The horopter and Spheres centers by bisector line when the depth δ grows. b) Hearing-Hildebrant deviation. c) Spherical horopter and the unit sphere, horopter circles by changing the azimuth of the intersecting plane π_i.d) Horopter depending on the azimuth angle κ.

depth perception that is stimulated by small amounts of retinal disparity is known as stereopsis (solid vision). The region around a fixation point is called the Panum's area which extends approximately $\pm$ 600 arc seconds on either side of the horopter. In a narrow range near of the horopter the stereopsis does not exist. That is due to very small disparities which are not enough to stimulate stereopsis. Empirical horopter measurements (even done using the $Nonius$ method) do not agree with the Vieth-Müller circle. There are two obvious reasons for this inconsistency either due to irregularities in the distribution of visual directions in the two eyes or a result of the optical distortion in the retinal image. For a perfect case it is expected that both retinas should be spherical, they should have symmetric distribution of local signs across nasal and temporal retinas, and both retinas should have the same size with same local sign geometry. The difference between the theoretical and the measured horopter under test distance is known as the Hearing-Hildebrant deviation, see Figure 1.b. There are various physiological reasons why the horopter can be distorted. We assumed that normal eye balls are round, but in the case of elongated eyes, like the eyes of myopes, the horopter could be distorted. Other cause of distortion is the asymmetric distribution of oculocentric visual distributions. In addition to a regional asymmetry in local signs in one eye, the distribution between the two eyes may not be congruent (correspondence problem), this may be another cause of horopter distortion. Asymmetric mapping from retina to the neocortex in both eyes also causes a deviation of the horopter from the Vieth-Müller circle. In this work we attempt to build an artificial binocular system. Deviations of the horopter in this artificial system will depend if the digital cameras fulfill the above summarized requirements for obtaining the Vieth-Müller circles. It is clear that modern cameras have limitations but they are not too serious. In the next subsections we explain our measures taken in order to avoid a distortion of the horopters. One important contribution of this work is to show that the horopter is naturally embedded in the unit sphere of the conformal geometric algebra. That is how we justify the introduction of the conformal geometric algebra as a modern and appropriate mathematical framework for building a binocular systems, remarkably enough to have certain degree of biological plausibility. The simple configuration of the horopter shown in Figure 1.a is nothing than a very naive geometric representation using polar coordinates of the geometric locus of the visual space. In contrast using the tools of conformal geometric algebra we can claim that binocular vision can be reformulated advantageously using an spherical retina. Now we show how we find the horopter in the sphere of conformal geometry. Actually we are dealing with a bunch of spheres intersecting the centers of the cameras L_C and R_C, see Figure 1.d. This is the pencil of spheres in the projective space of spheres. Note that the L_C and R_C cameras centers are Poncelet points. Since a stereo system only sees in front of it, we consider the spheres emerging towards the front. When the space locus of objects expands, the centers of the spheres move along the bisector line of the stereo rig, this is when the depth δ grows, see Figure 1.a. From now onwards we will use the term horopter sphere rather than the horopter circle, because when we change the azimuth of the horopter circle we are simply selecting a different circle of a particular horopter sphere s_i, see Figure 1.c. As a result we can consider that all the points of the visual space are lying on the pencil of the horopter spheres. Let us translate this description in terms of equations of the conformal geometric algebra. We call the unit horopter sphere s_0 the one which has as center the egocenter of the stereo rig, see Figure 2 and using equation 10,

$$s_0 = p - \frac{1}{2}\rho^2 e_\infty = \mathbf{c}_0 + \frac{1}{2}(\mathbf{c}_0^2 - \rho^2)e_\infty + e_0, \qquad (16)$$

where its center (egocenter) is attached to the true origin of space of the conformal geometric algebra and the radius is the half of stereo rig length $\rho_0 = \frac{1}{2}|L_C - R_C|$. The center $\mathbf{c}_i$ of any horopter sphere s_i moves towards the point at infinity as $\mathbf{c}_i = \mathtt{c}_i + \frac{1}{2}(\mathtt{c}_i^2)e_\infty + e_0$, where $\mathtt{c}_i$ is the Euclidean 3D vector. Thus we can write the equation of the sphere s_i as $s_i = \mathtt{c}_i + \frac{1}{2}(\mathtt{c}_i^2 - \rho_i^2)e_\infty + e_0$, where the radius is computed in terms of the stereopsis depth $\rho_i = \frac{1}{2}(1+\delta)$. Consider the figure of the model for visual human system in Figure 1.d, we see that the horopter circles lye on a pencil of planes π_i. We can obtain the same circles z_i simply by intersecting in our conformal model such pencil of planes with the pencil of

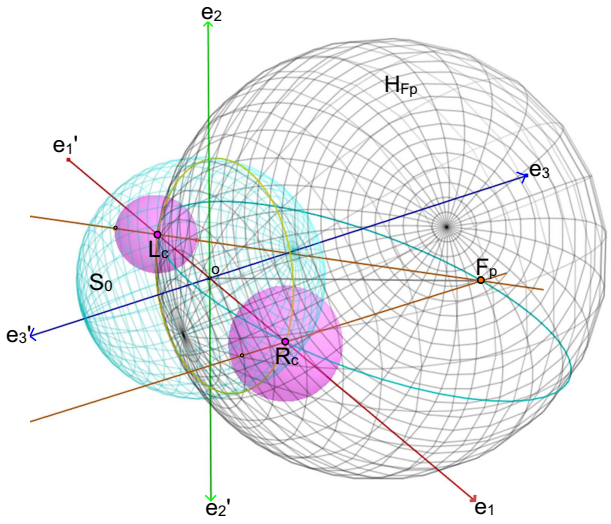

Fig. 2. Conformal horopter configuration, Left Camera center L_c, Right Camera center R_c and Fixation Point F_p define a Circle which by means of varying κ defines a family of spheres or Horopter Spheres

tangent spheres as is depicted in Figure 1.c. The intersection is computed using the meet operation of the duals of the plane and sphere and taking the dual of the result as $z_i = \pi_i \wedge s_i$. Now, taking the meet of any couple of horopter spheres we gain a circle which lies on the front parallel plane with respect to the digital cameras common plane $z = s_i \wedge s_j$. Later on taking the meet of this circle with the unit horopter we regain the Poncelet points L_C and R_C which in our terms is called point pair $\mathbf{PP}_{LR} = \mathbf{z} \wedge \mathbf{s}_0 = \mathbf{L} \wedge (\mathbf{s}_0^*)$, note that the second part of the equation computes the point pair wedging the dual of sphere s_0^* with the line crossing the camera centers L_C and R_C.

If we further consider the Figure 1.c., the intersecting plane π_i cuts the horopter spheres generating geometric locus on the plane as depicted in Figure 1.c-d. These horopter circles fulfill an interesting property. If one takes an inversion of all horopter circles with centers on the line l we get the radial lines of the polar diagram, see at the right in Figure 4.a. Now, since the plane π_i (by varying angle κ) intersects the family of horopter spheres producing the horopter circles of Figure 4.a whose inverse is a 2D log-polar diagram, we can conclude that the inverse of the arrangement of horopter spheres and Poncelet points is equivalent a 3D log-polar diagram, as depicted in Figure 4.b. To understand this better, lets us take any radial line of the 2D log-polar diagram and express it in conformal geometric algebra $\mathbf{L} = \mathbf{X} \wedge \mathbf{Y} \wedge e_\infty$. Now, applying an inversion to this line we get a circle, i.e. $z = e_4 \mathbf{L} e_4$. Note that this inversion is implemented as a reflection on e_4. The 3D log-polar diagram is an extraordinary result, because contrary to the general belief that conformal image processing takes places in 2D log-polar diagram, we can consider that the visual processing rather takes place in a 3D log-polar diagram. This claim is novel and it is promising, because this framework can be used for 3D flow estimation as opposite to the use of one view or even an arrangement of two log-polar cameras. In this paper we use our conformal model in a real binocular head which we will utilize for an humanoid, or as an intuitive vision-based man-machine interface and also for advanced 3D automated visual inspection.

B. Building the conformal horopter using a binocular head

A half-body humanoid is being built in order to research models and algorithms for perception action systems based on conformal geometric algebra, this system includes a robotic arm, hand, neck (pan-tilt unit) and stereoscopic vision (see Figure 3.a-b). The front parallel cameras system provides an

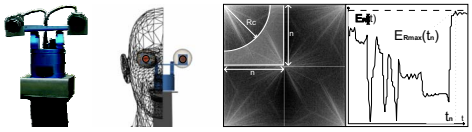

Fig. 3. a) Humanoid's pan-tilt unit and stereoscopic vision system. b) Humanoid's virtual reality scene. c) High frequency region limited by the cut-off radius R_c and half of the image size n. d) Maximal energy amount $E_R(t)$ in high frequency region at time t_n.

excellent platform to implement the conformal horopter (see Figure 4.c). In order to support the assumptions made upon the model, we use an effective technique to adjust focal distances of both cameras. Since both cameras are the same model and have the same lenses mounted, we could therefore assume equal image resolution; in terms of human vision parameters this would be taken as equal retina size on both eye balls. This is a very important issue to assure so that the image and geometric process will be done in a non degenerated horopter. So priori standard camera calibration, the focal distance is set as follows. First we capture a gray scale image $I_l(x, y, t_0)$ at time t_0 on the left camera, then we map the image into its Fourier representation $F_l(u, v, t_0) = \mathcal{F}\{I_l(x, y, t_0)\}$. Hence, the spectral density $P_l(u, v, t_0) = |F_l(u, v, t_0)|^2$ is computed in order to determine the energy distribution in the bidimensional signal. The high frequency region could be thought as the zone which extends beyond certain cut-off radius R_c, i.e. where the frequency variable u or v (or perhaps both) represents the high frequency components of the image, see Figure 3.c. The contribution of a certain

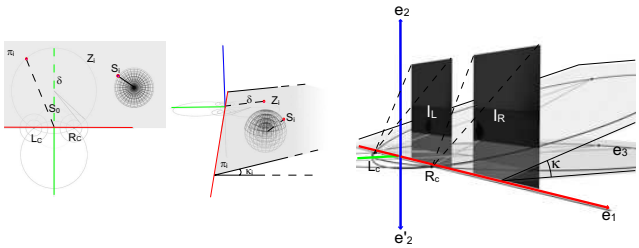

Fig. 4. a) Left side:Log-polar representation of visual space b) Center:Log-polar space and the azimuth κ angle. c)Rightside: Nodal points L_C-R_C (camera's centers), image planes I_L-I_R, and the azimuth angle κ showing the epipolar pencil of planes where the Vieth-Müller circles yields.

component $P_l(u, v, t)$ to the zone is determined (weighed to avoid rippling) by $B(i, j, R_c) = 1 - e^{-\sigma(i^2+j^2)R_c/2}$. This zone

implies all the components of the signal that constitute the corners or borders in space domain, features found in a well-focused camera. Since the energy amount in this region at certain time $E_R(t)$ is related to the sharpness of the image we calculate it as discrete weighed integration $E_R(t_0) = \sum_{i=1}^{n}\sum_{j=1}^{n} B(i,j,R_c)P(i,j,t_0)$, where n means half of the width or height of the square image, then a second image at time t_1 is processed in the same way. While these calculations take place we physically adjust the focal length of the lens until the maximal $E_{RMax}(t_n)$ is reached see Figure 3.d. Once the left camera has gone through this stage we do the same with the right one. Finally since we do not only wish to get the best possible focus for each camera, but also to make the system evenly focused, the strategy consists in establishing a subwindow $W_L(x,y,R_s) = [(x-R_s) \leq x_i \leq (x+R_s)] \times [(y-R_s) \leq y_i \leq (y+R_s)]$ in the left image (such that its content appears in the 3D field of view, so it can be found in both images), and apply this subwindow as correlation kernel with the right image in order to find the best match. This was implemented with the bidimensional convolution in frequency domain, taking into account that the correlation kernel will be the left subwindow, but horizontally and vertically flipped. This Kernel was improved for our purposes with an edge detector filter (3x3 pixels).

Later on, we calibrated the stereo rig with a well-known method from [3]. Uniform temporal distribution of features on images is an important restriction which needs to be tackled, in order to support this assumption our binocular system controls the frame rate and synchronization at every single capture based on common computational thread schemes. Spatial distribution of features is assured with a full camera calibration including lenses distortion (radial-tangential) and projective compensations. The disparities found in images are handled as head-centric iso-disparities surfaces. These are the meshes that supports stereo matching, and more over scene reconstruction. Since off-line calibration procedure has been finished, the next stage consists in computing those iso-disparities surfaces using a multiresolution algorithm see Figure 5, this method is inspired on *census mapping* for correspondence estimation, however our algorithm uses an central pixel difference. This process has been accelerated by a set of constraints (ordering, uniqueness, disparity limit, disparity continuity, etc.) [2], [6]. When dense mesh reconstruction is wished a median-like filter must be applied to distinguish those outliers which were not taken by the disparity limit constraint. This median-like filter has to consider only those pixels with non zero disparity and in addition the value set to every filtered pixel will depend on both the mean and median of the neighborhood. The variation of azimuth angle κ generates a pencil of planes which could be seen as the epipolar plane whose intersections with the images planes are the scan lines of the images (see figure 4.c), this is possible because the epipolar calibration has been done during the wrapping phase (where lens distortion and center of the cameras are compensated) of the on-line 3D scene mesh generation. Finally the 3D mesh of the field of view is formed by two sets of vertices (conformal 5D points), one set on the unit sphere whose center is the stereo rig origin and the other set at the corresponding 3D scene points, this data is properly encoded in conformal points.

Fig. 5. Disparity Map by means of a Multiresolution Algorithm, where scan lines correspond to the intersections between the pencil of epipolar planes and the image planes.

Due to the geometric nature of our approach, the usage of geometric primitives (as planes, lines, etc.) together with the incidencde algebra provides us with a powerful tool-box for further applications, however until this point the content in the visual space has been encoded with conformal points. The idea is to find these geometric primitives from the mesh in such a manner that effects of noise and quantization induced by the digital images could be diminished. In this way we address an intuitive geometric approach for visual space perception under uncertainty.

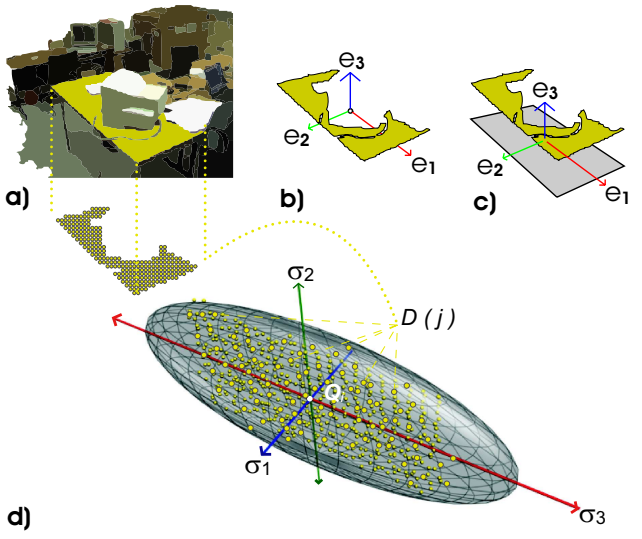

Fig. 6. a) Segmented Image for geometric rectification based on plane-patch fitting b) Selected Patch and its Centroid c) Plane Fitting based on eigen vectors from Covariance Matrix M_i d)Ellipsoid represented by covariance matrix M_i where axes are obtained by the eigenvectors from $eig(M_i)$

A technique to do this in laser range data has been use by [9],to improve the performance and quality (on stereo images) we use the patches in the images which may be suitable to be a certain geometric primitive, ie. in the case of the plane the image patch will be similar in texture or color, this

similarity could be determined by a segmentation phase using well known algorithms [8], once the image segmentation is done, then it is possible to define a list of conformal points from the iso-disparity mesh which correspond to a particular image patch i, this list is denoted by $D_i(j)$ where j is the index of a particular conformal point, the size of the list is m_i, then the 3D centroid Q_i of the conformal points within the list is calculated see Figure 6. After that the plane fitting phase is applied in every patch using a covariance matrix W_i [9] as:

$$H_i = \frac{1}{i}[\sum_{j=1}^{m_i} D_i(j)] \tag{17}$$

$$Q_i = (H_i \cdot e_1)e_1 + (H_i \cdot e_2)e_2 + (H_i \cdot e_3)e_3 \tag{18}$$

$$_{p,q} = \sum_{j=1}^{m_i} \{(D_i(j) \cdot e_p) - (Q_i \cdot e_p)\}\{(D_i(j) \cdot e_q) - (Q_i \cdot e_q)\} \tag{19}$$

$$W_i = \begin{bmatrix} _{1,1} & _{1,2} & _{1,3} \\ _{2,1} & _{2,2} & _{2,3} \\ _{3,1} & _{3,2} & _{3,3} \end{bmatrix}$$

then we calculate the eigen values (σ_1, σ_2 and σ_3) and eigen vectors (ν_1, ν_2 and ν_3) from W_i, where the eigen vector ν_1 from the smallest eigen value σ_1 represent the normal of the plane, so from equation 13 $\pi_i = \nu_1 + |Q_i|_\infty$, in this fashion we use this geometric primitive for space rectification, this is indeed done by means of intersecting planes ($l = \pi_a \wedge \pi_b$) to get the lines which describe boundaries for the patch, among other geometric corrections.

C. Applications for humanoid vision

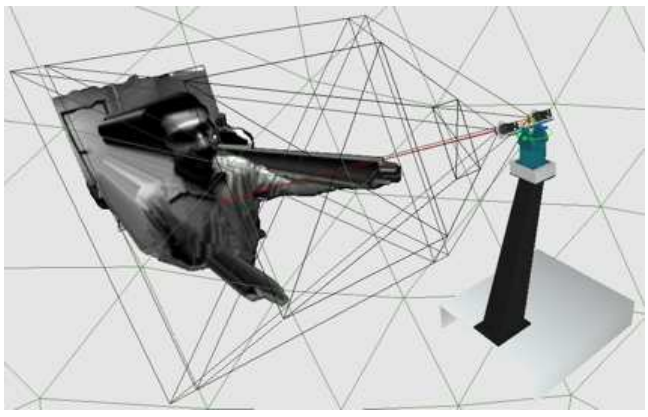

Fig. 7. 3D Scene Reconstruction, depth segmentation and Ego-Sphere visualization in virtual reality for Human computer interaction, using conformal horopter.

The conformal model has been used to build an application where a scene reconstruction and modeling has been done, this data is used to segment elements in the field of view bases on its depth (in a multiresolution manner). More information (color skin, shape, etc.)is used to estimate the user pose or gesture. Once this pose is know we can define assets in the 3D virtual world, in such a away that if the user touches this asset some command is dispatched see Figure 7.

IV. Conclusions

In this work we introduced a novel conformal model for human like vision. The standard concept of horopter circles is extended to a horopter spheres which leads to a 3D log-polar representation of the visual space. Our model appears very suitable to build a powerful fused stereoscopic system which can be used for perception in humanoids, intuitive man-machine interfaces and advanced 3D automated visual inspection.

References

[1] R. Mandelbaum, L. McDowell, L. Bogoni, B. Reich, M. Hansen. Real-time stereo processing, obstacle detection, and terrain estimation from vehicle-mounted stereo cameras. In Proc. of the 4th IEEE Workshop on Applications of Computer Vision (WACV'98), pp. 288-294, 1998.

[2] M. Pollefeys, S. Sinha. Iso-disparity surfaces for general stereo configurations. T. Pajdla and J. Matas (Eds.), Computer Vision - ECCV 2004 (European Conference on Computer Vision), LNCS Springer-Verlag, Vol. 3023, pp. 509-520, 2004.

[3] Z. Zhang. Flexible Camera Calibration by Viewing a Plane from Unknown Orientations. Seventh International Conference on Computer Vision (ICCV'99) - Volume 1, pp. 666-672, 1999.

[4] S. Steinman. Binocular Vision Module-The Empirical Horopter, Addison-Wesley, 1994.

[5] C. Capurro, F. Panerai and G. Sandini. Dynamic Vergence Using Log-Polar Images. International Journal of Computer Vision, Volume 24, No. 1, pp. 79-94, 1997.

[6] M. Pollefeys, S. Sinha. Iso-disparity surfaces for general stereo configurations. T. Pajdla and J. Matas (Eds.), Computer Vision - ECCV 2004 (European Conference on Computer Vision), LNCS, Springer-Verlag, Vol. 3023, pp. 509-520, 2004.

[7] Bayro-Corrochano E. Robot perception and action using conformal geometric algebra. In Handbook of Geometric Computing, Applications in Pattern Recognition, Computer Vision, Neuralcompouting and Robotics, Ed. Eduardo Bayro-Corrochano, Chap. 13, Springer Verlag, Hedeilberg, pp. 405-460, 2005.

[8] D.Comaniciu and P.Meer. Mean shift: A robust approach toward feature space analysis. IEEE Trans. Pattern Anal. Machine Intell , 24 , pp. 603-619, 2002.

[9] J. Castao, E. Zalama and J. Gmez. Reconstruction of Three Dimensional Models of Environments with a Mobil Robot. In Proc. of the International Conference on Robotics and Automation, ICRA'2003, New Orleans, 2003.